Application of XTRAN3S and CAP-TSD to Fighter Aircraft

D. M. Pitt,* D. F. Fuglsang,† and D. V. Drouin†
McDonnell Douglas Corporation, St. Louis, Missouri 63166

Two unsteady transonic small-disturbance (TSD) codes, XTRAN3S and CAP-TSD, were used to perform aeroelastic analyses of four fighter aircraft configurations. The XTRAN3S code was used for a wing-alone analysis of the F-15 and F/A-18 aircraft, whereas the CAP-TSD code, with its more flexible geometric modeling capability, was used to analyze a canard, wing, and tail arrangement of the F-15 S/MTD and a wing, launcher, and tip missile arrangement of the F/A-18. Static and dynamic aeroelastic calculations were performed using both the linear and nonlinear forms of the small-disturbance equation. Comparisons are made between the F-15 and F/A-18 wing-alone flutter results and those from a linear flutter analysis computed using doublet lattice aerodynamics. These comparisons show good agreement for the linear aerodynamic TSD solutions but significant changes in the flutter speed for the nonlinear aerodynamic TSD solutions. Comparisons were also made for the canard/wing/tail and the wing/launcher/tip missile configurations with the corresponding wing-alone configurations to assess the effects of multiple lifting surfaces and tip stores on flutter.

Nomenclature

C_L = total lift coefficient
C_l = section lift coefficient
C_p = pressure coefficient
$C_{(1/4)m}$ = section moment coefficient about 1/4 chord
g = structural damping coefficient
M_∞ = freestream Mach number
q_i = generalized coordinate of motion for mode i
q_∞ = freestream dynamic pressure
t = nondimensional time
V_∞ = freestream velocity
Wt = nondimensional time step size
α = angle of attack, deg
α_m = mean angle of attack, deg
η = fractional semispan along planform
ω,ω_n = natural circular frequency
ω_d = damped circular frequency

Introduction

THE purpose of this research was to study the effects of nonlinear aerodynamics on the transonic aeroelasticity of realistic fighter geometries. Because of the complex nature of the aeroelastic problem, the highly coupled interaction between the aerodynamic forces and the flexible structure, traditional methods of numerical analysis have been restricted to linear mathematical models. However, within the transonic speed range, the assumption of linear aerodynamics can introduce large errors into the aeroelastic calculations.

Two unsteady transonic small-disturbance (TSD) codes, XTRAN3S and CAP-TSD,[1,2] were used to perform an aeroelastic analysis of four fighter aircraft configurations. The XTRAN3S code was used for the wing-alone analysis of the F-15 and F/A-18 aircraft, whereas the CAP-TSD code with its more flexible geometric modeling capability was used to analyze the canard, wing, and tail arrangement of the F-15 S/MTD and the wing, launcher, and tip missile arrangement of the F/A-18. Both static and dynamic aeroelastic calculations were performed using the linear and nonlinear forms of the small-disturbance equation. The F-15 and F/A-18 wing-alone flutter results were compared with those from a traditional linear flutter analysis computed using doublet lattice[3] aerodynamics. Comparisons were also made for the canard/wing/tail and the wing/launcher/tip missile configurations with the corresponding wing-alone configurations to determine the effects of multiple lifting surfaces and tip stores on transonic flutter. The work reported here constitutes a portion of the more extensive research study of Ref. 4.

Time-Marching Aeroelastic Analysis

The XTRAN3S and CAP-TSD codes perform an aeroelastic analysis by coupling a finite difference formulation for the aerodynamics to the aircraft structural equations of motion.

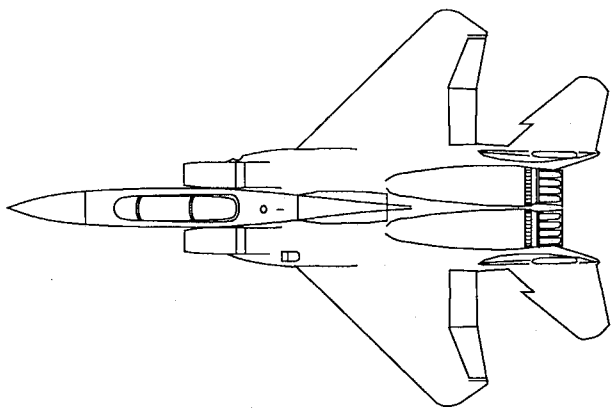

Fig. 1 Planform view of the F-15 aircraft.

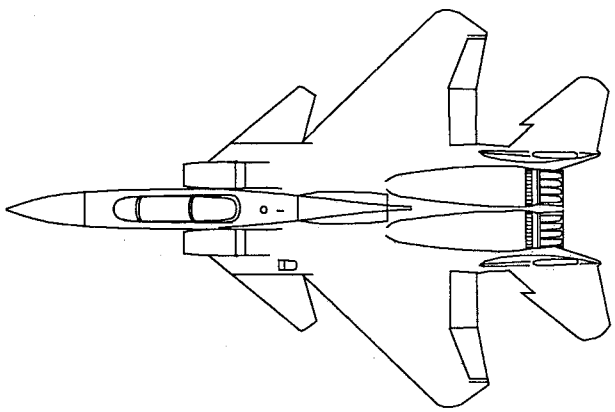

Fig. 2 Planform view of the F-15 S/MTD aircraft.

Presented as Paper 90-1035 at the AIAA/ASME/ASCE/AHS/ASC 31st Structures, Structural Dynamics and Materials Conference, Long Beach, CA, April 2-4, 1990; received May 12, 1990; revision received Oct. 18, 1990; accepted for publication Oct. 18, 1990.

*Senior Technical Specialist, McDonnell Aircraft Company, P. O. Box 516. Associate Fellow AIAA.
†Senior Engineer, McDonnell Aircraft Company. Member AIAA.

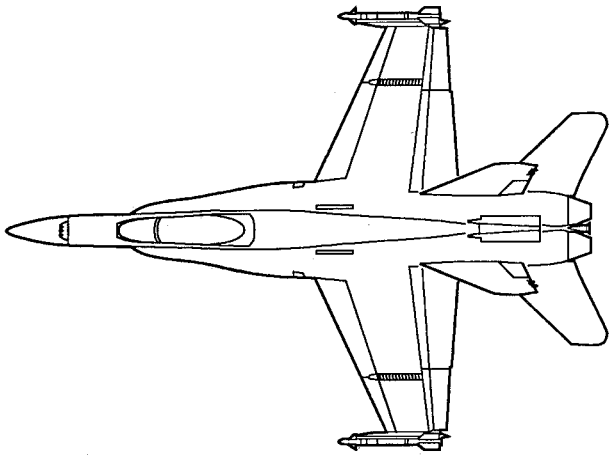

Fig. 3 Planform view of the F/A-18 aircraft.

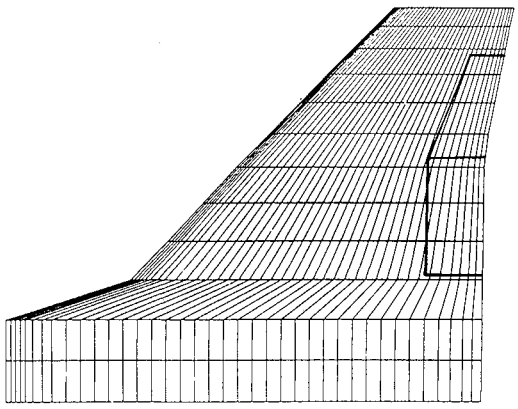

Fig. 4 F-15 XTRAN3S wing with computational grid.

The equations of motion are formulated in the time domain and are based on the aircraft natural vibration modes. The XTRAN3S code solves the unsteady transonic small-disturbance equation using an alternating-direction implicit (ADI) finite difference algorithm,[1] whereas the CAP-TSD code uses a time-accurate approximate factorization (AF) algorithm[2] applied to the TSD equation. The aeroelastic equations of motion are integrated in time within the XTRAN3S code using an Adams-Moulton predictor-corrector method as described in Ref. 5, whereas the CAP-TSD code uses a modified state transition matrix structural integrator implemented as a predictor-corrector procedure described in Ref. 6.

XTRAN3S and CAP-TSD Code Application Results

Results are presented for four aircraft configurations as applications of the XTRAN3S and CAP-TSD aeroelastic codes. The four configurations are 1) the F-15 wing; 2) the F-15 S/MTD wing, canard, and tail; 3) the F/A-18 wing; and 4) the F/A-18 wing with tip missile. The XTRAN3S code was used to analyze the F-15 and F/A-18 wings, whereas the CAP-TSD code was used to analyze the F-15 S/MTD and F/A-18 wing with tip missile. Planform views of the aircraft are shown in Figs. 1-3.

XTRAN3S Calculations for the F-15

The F-15 wing with unclipped tip, trailing-edge flap, and aileron has an aspect ratio of 3.01, a leading-edge sweep of 45 deg, and a taper ratio of 0.25. The airfoil section of the F-15 wing is a modified NACA64A series that varies in thickness from 5.9% at the root to 3% at the wingtip. The wing planform as modeled for the analysis is shown in Fig. 4 along with XTRAN3S grid point distribution on the surface.

A modal reduction study[4] was performed using doublet lattice aerodynamics to reduce the number of wing vibratory modes from 25 to 3. These modes, calculated from a finite element model that was correlated with measured ground vibration test data, predict the basic flutter mechanism for the F-15 wing.

A static aeroelastic analysis was performed using both linear and nonlinear XTRAN3S aerodynamics coupled with the three-mode vibration model of the structure. The conditions used in the analysis were $M_\infty = 0.9$, $\alpha_m = 0.08$ deg, and $q_\infty = 25.9$ psi. (This is the linear doublet lattice flutter dynamic pressure.) Perspective views of the deformed wing for both the linear and nonlinear static aeroelastic solutions are shown in Figs. 5 and 6, respectively. The deformed shape for the nonlinear case has a larger amount of wing bending and wing torsion than the linear case. The tip rotation angle for the linear case was computed to be approximately 6.3 deg (leading edge down), whereas in the nonlinear case, it was computed to be 8.6 deg.

For the dynamic aeroelastic analysis of the F-15 XTRAN3S model, solutions were computed using both the linear and full nonlinear formulation of the small-disturbance equation. All calculations were performed at a freestream Mach number of $M_\infty = 0.9$ and a mean wing angle of attack of $\alpha_m = 0.08$ deg. Only the freestream velocity V_∞ and dynamic pressure q_∞ were varied between cases. The time step size and the number of iterations were selected to allow at least three cycles of the lowest frequency mode to be computed while maintaining a minimum of 200 steps per cycle of the highest frequency mode. Each of the dynamic aeroelastic solutions produced three transient responses, one for the generalized displacement of each modal motion. These responses were curve fit using a damped sine wave modal decomposition method to determine their damping and frequency. The component damping is used to indicate whether the dynamic pressure for the given case was above or below the flutter point.

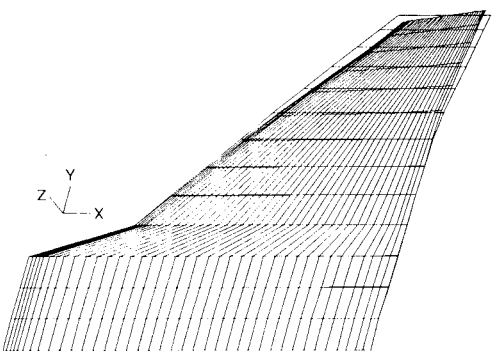

Fig. 5 Perspective view of the F-15 XTRAN3S static aeroelastic solution computed using the linear TSD equation.

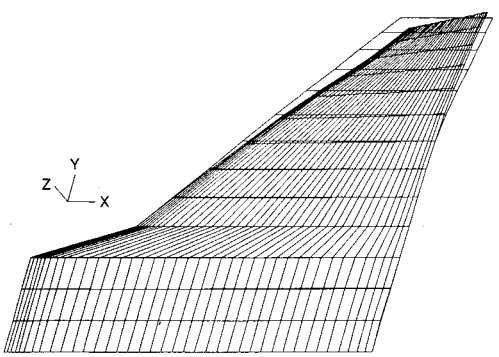

Fig. 6 Perspective view of the F-15 XTRAN3S static aeroelastic solution computed using the nonlinear TSD equation.

Results from a sample dynamic aeroelastic solution computed using linear XTRAN3S aerodynamics are shown in Fig. 7. The conditions used for the calculation were $V_\infty = 950$ kt and $q_\infty = 21.2$ psi. The figure contains the time histories for the three generalized displacements and clearly shows converging transients, indicating a stable solution below the flutter point. Alternately, the solution computed using nonlinear aerodynamics for the same flight conditions is shown in Fig. 8. The generalized displacement time histories show diverging (growing) response for mode 1, indicating an unstable response above the flutter point.

The stability of the system can also be examined through a phase plane representation of the response. Figure 9 shows a

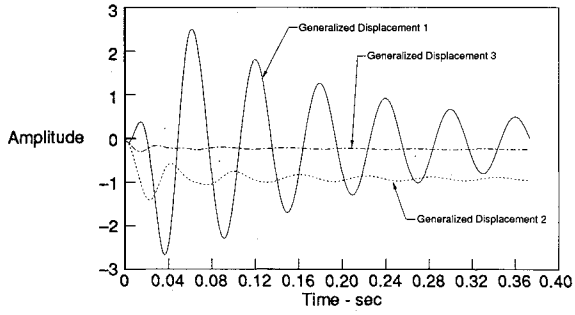

Fig. 7 F-15 XTRAN3S time history responses for the generalized displacements computed using the linear TSD equation.

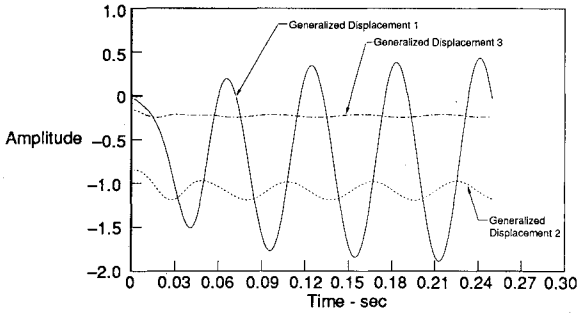

Fig. 8 F-15 XTRAN3S time history responses for the generalized displacements computed using the nonlinear TSD equation.

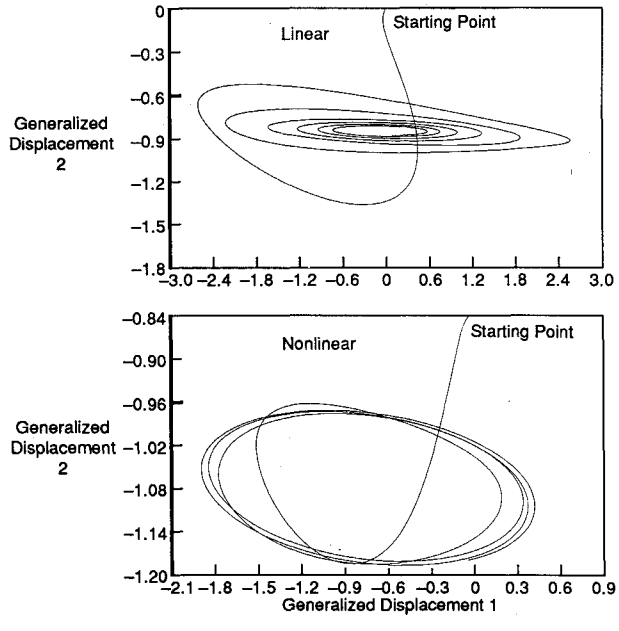

Fig. 9 F-15 XTRAN3S phase plane plots for the first and second generalized displacements computed using the linear and nonlinear TSD equation.

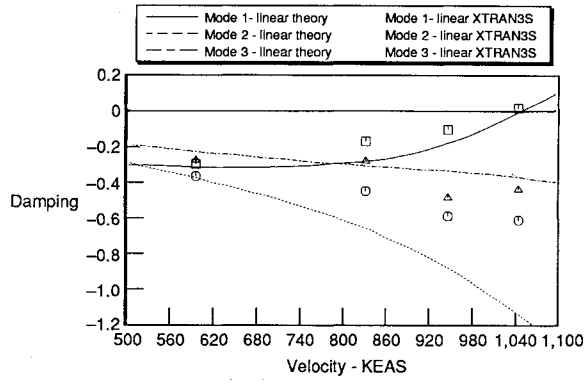

Fig. 10 *V-g* comparison plot between linear theory computed using doublet lattice aerodynamics and the F-15 XTRAN3S values computed using the linear TSD equation.

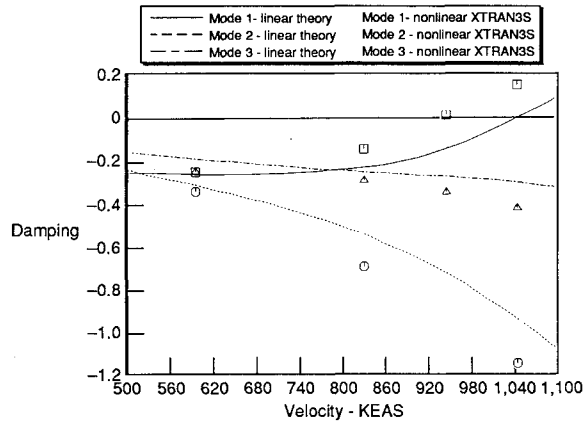

Fig. 11 *V-g* comparison plot between linear theory computed using doublet lattice aerodynamics and the F-15 XTRAN3S values computed using the nonlinear TSD equation.

plot of the first generalized displacement vs the second generalized displacement for the transients of Figs. 7 and 8. As discussed earlier, the linear aerodynamic solution is stable, which, in the phase plane plot, is indicated by the inward spiraling curve. The instability of the nonlinear aerodynamic solution is indicated by the outward spiraling curve.

The dynamic aeroelastic behavior of this configuration (for the stated Mach number and angle of attack) is summarized by the damping vs velocity plots in Figs. 10 and 11. The modal damping values extracted from the transients of the generalized displacements are plotted in the figures along with baseline results computed from a *P-k* linear flutter analysis using doublet lattice[3] aerodynamics. In comparing the XTRAN3S damping values and those from the *P-k* analysis, reasonable quantitative agreement can only be seen when the modes are not heavily damped. Heavily damped modes are difficult to curve fit and are easily contaminated by numerical and/or initial condition transients introduced into the calculations. Qualitatively, however, both the *P-k* and XTRAN3S results show similar modal trends as mode 1 flutters and modes 2 and 3 become more heavily damped with increasing velocity. The figures indicate a linear flutter speed of approximately 1040 kt and a nonlinear flutter speed of approximately 945 kt obtained by interpolating between the XTRAN3S solutions. This is compared to a flutter speed of 1050 kt obtained using doublet lattice aerodynamics.

CAP-TSD Calculations for the F-15 S/MTD

The second configuration is the wing, canard, and tail arrangement for the F-15 S/MTD. The configuration was modeled in CAP-TSD with three lifting surfaces and included the trailing-edge flap and aileron of the wing. A planform

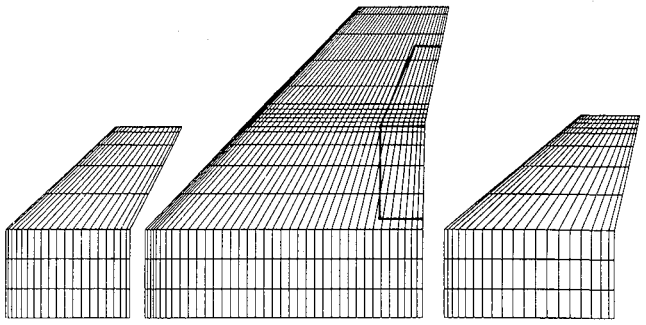

Fig. 12 CAP-TSD F-15 S/MTD canard, wing, and tail arrangement with computational grid.

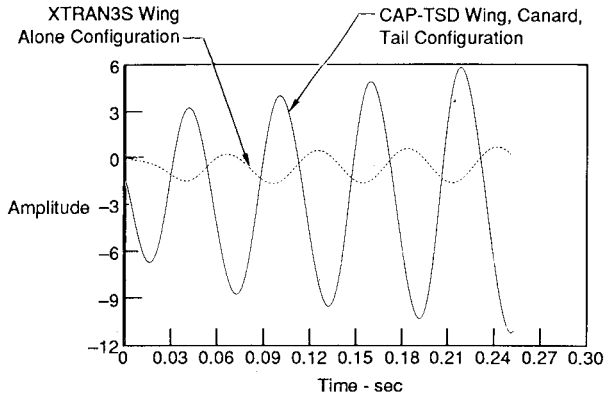

Fig. 13 CAP-TSD and XTRAN3S time history responses for the first generalized displacement computed using the nonlinear TSD equation.

view of the simplified model as used for the calculations is shown in Fig. 12. The grid point distributions on the lifting surfaces are as shown in the figure.

To study how the aerodynamic effects of multiple lifting surfaces influence aeroelastic response, only the wing in this configuration was modeled as a flexible structure. The canard and tail were treated as rigid structures to provide only aerodynamic interference effects. To further simplify the analysis, the same structural representation that was used for the F-15 XTRAN3S calculations was also used for the S/MTD.

A sample dynamic aeroelastic solution computed using nonlinear aerodynamics is presented in Fig. 13. The freestream conditions were $M_\infty = 0.9$, $\alpha_m = 0.08$ deg, $q_\infty = 21.2$ psi, and $V_\infty = 950$ kt. These conditions were chosen because they produced the unstable response in the F-15 XTRAN3S calculations. Within the figure are plotted the time histories of the first generalized displacement for both the three-lifting-surface S/MTD configuration and the F-15 wing-alone configuration (see Fig. 8). The effect of the canard and tail is to induce a higher amplitude response that diverges at a slightly faster rate. This flutter trend is contrary to what was predicted using linear doublet lattice aerodynamics. It is also seen that the mean value about which the responses oscillate changes considerably between the wing-alone and wing, canard, and tail configurations. This mean value represents the contribution of the first vibratory mode to the static aeroelastic solution if no oscillations were present.

XTRAN3S Calculations for the F/A-18

The third configuration is the F/A-18 wing with leading- and trailing-edge control surfaces. The wing has an aspect ratio of 3.5, a leading-edge sweep of 26.7 deg, and a taper ratio of 0.348. The airfoil section of the F/A-18 wing is a modified NACA65A series that varies in thickness from 5% at the root to 3.5% at the wingtip. In addition, the wing has a negative 4-deg linear twist starting at the wing fold mechanism, at a semispan location of $\eta = 65\%$ to the wingtip at $\eta = 100\%$. The XTRAN3S wing grid used in the analysis is shown in Fig. 14.

The wing was modeled structurally using five vibration modes. The modes were chosen to simulate an observed wing/store/tip missile limit cycle oscillation mechanism for the F/A-18 wing. It is noted that the vibratory modes contain the effects of the mass of a tip missile and under wing stores even though their aerodynamic influence could not be included in the aeroelastic analysis.

Results from a dynamic aeroelastic analysis for the F/A-18 wing computed using nonlinear aerodynamics are presented in Fig. 15. The calculations were performed at $M_\infty = 0.8986$ and $\alpha_m = 0.44$ deg, with the results shown for two different velocities, $V_\infty = 748.6$ and 1122.9 kt. Within the figure are time history plots of the third generalized displacement along with the associated component plots computed from the damped sine wave decomposition of the generalized displacements. The results show that as freestream velocity is increased an unstable response is obtained. Based on these and other aeroelastic calculations, the nonlinear flutter speed of 1085 kt was obtained. This is compared with a flutter speed of 970 kt computed when using linear XTRAN3S aerodynamics or a flutter speed of 940 kt computed when using doublet lattice aerodynamics.

The F/A-18 wing total lift coefficient time history for the nonlinear flutter point at $V_\infty = 1122.9$ kt is presented in Fig. 16. The lift is a divergent sinusoidal oscillation about a mean lift coefficient of 0.015. Two specific iterations are labeled as minimum and maximum lift on the time history. Within Fig. 16 are comparison plots of the wing upper and lower surface C_p distribution at the time of minimum and maximum lift at an inboard, midspan, and wingtip span location. An important feature within the figure is the increasing variation between the minimum and maximum lift pressure distributions when proceeding from root to tip span locations. This is to be expected since the largest wing deformation occurs at the wingtip. Also seen in the figure is a weakening of an upper surface shock and the emergence of a strong lower surface shock when proceeding from the root to the wingtip.

CAP-TSD Calculations for the F/A-18 Wing with Tip Missile

The fourth configuration is the F/A-18 wing with launcher and tip missile. For the CAP-TSD analysis, certain geometric simplifications had to be made to the aerodynamic model of the missile. First, the tip missile body was modeled as a lifting surface with airfoil ordinates representing the missile cross-

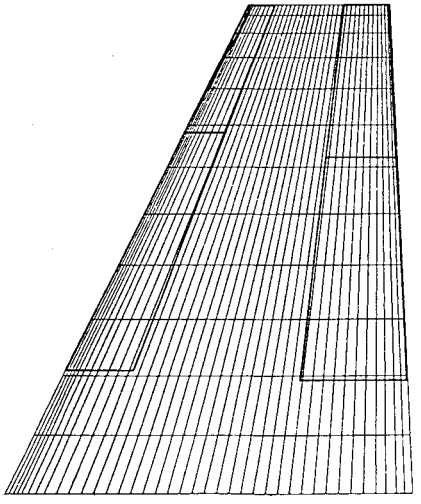

Fig. 14 F/A-18 XTRAN3S wing with computational grid.

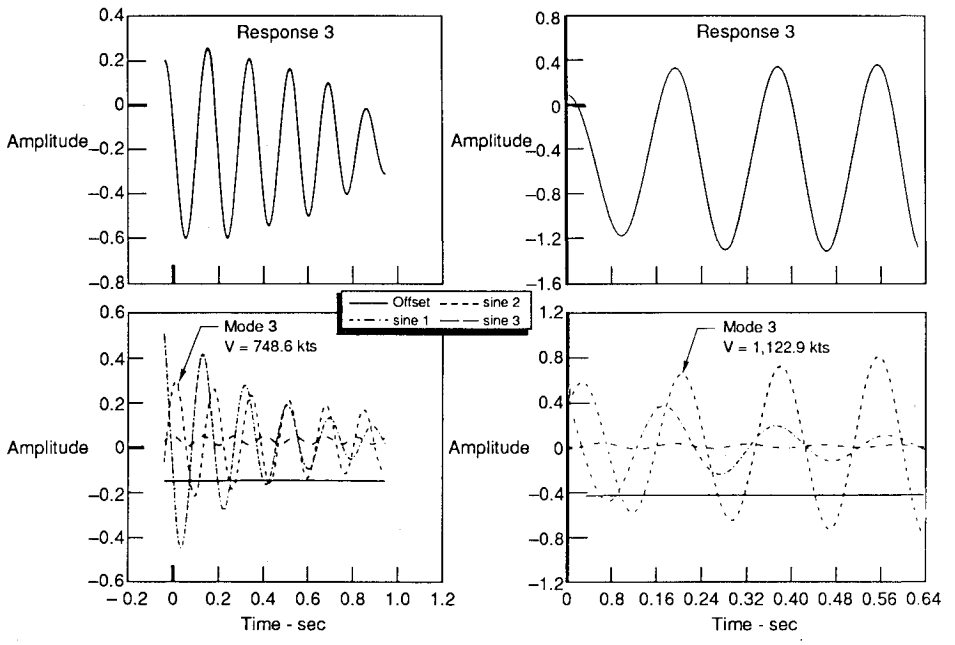

Fig. 15 XTRAN3S time history response and modal components for the third generalized displacement computed using the nonlinear TSD equation.

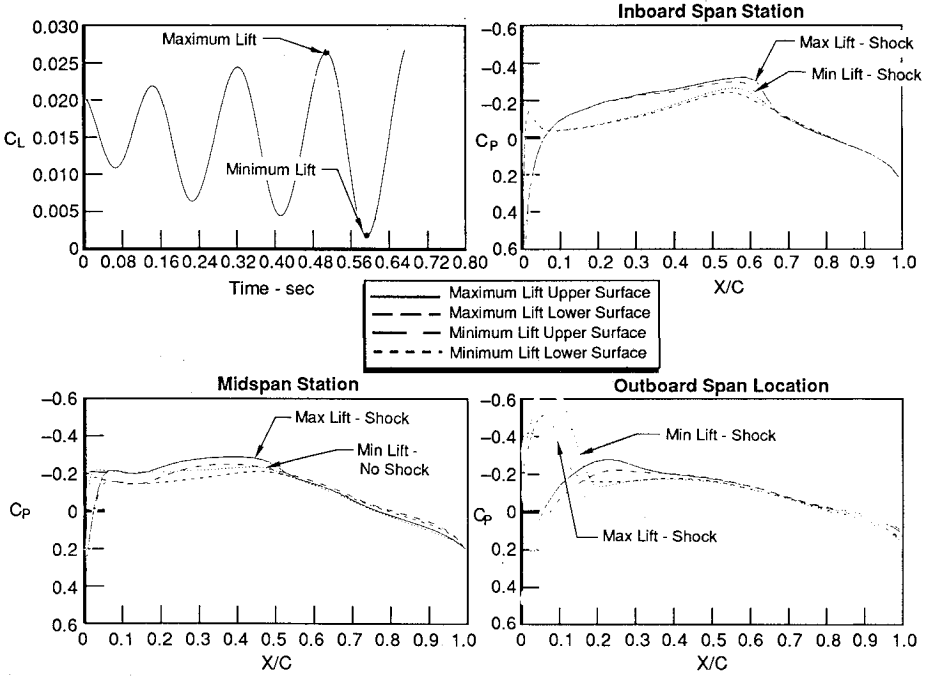

Fig. 16 F/A-18 XTRAN3S total wing C_L time history and chordwise C_p distribution computed using the nonlinear TSD equation.

sectional shape. This was necessary so that the unsteady body pressures would be integrated for generalized force calculations. Also, it was not possible to model the missile's forward and aft fins at their normal 45-deg inclination, and so they were rotated to appear in the vertical and horizontal plane. This resulted in four rectangular vertical fins and two horizontal fins on the missile. Slight compromises were made to fin planform shape. A planform view of the F/A-18 wing and tip missile grid is presented in Fig. 17.

For the structural model of this configuration, the same five vibrational modes used for the F/A-18 wing XTRAN3S calculations were used for the wing/launcher/tip missile calculations in CAP-TSD except that now the contribution of the launcher, missile body, and fins is included in the evaluation of the generalized aerodynamic forces. By retaining the same structural model, the effects of the tip missile on the aeroelastic response of the wing can be more closely examined.

CAP-TSD rigid static aerodynamic calculations were performed for both the wing-alone and wing/launcher/tip missile configurations. The conditions were $M_\infty = 0.8986$ and $\alpha_m = 0.4397$ deg. Figure 18 contains plots of computed section C_l and $C_{(1/4)m}$ (the spanwise locations have been nondimensionalized by the reference chord). In the figure, the full (wing, launcher, and tip missile) configuration predicts a lower section C_l than the wing-alone case. Also, the section pitching moment $C_{(1/4)m}$ for the full configuration results in lower values inboard and larger (more negative) values at the tip. The changes in the spanwise loads and moments are due to the fact that the tip missile and launcher are twisted down 4 deg to match the geometric twist of the wingtip.

The static aeroelastic solutions computed for the two configurations just mentioned are shown in Fig. 19. The conditions were $M_\infty = 0.8996$ and $\alpha_m = 0.4397$ deg. The figure contains plots of section C_l and $C_{(1/4)m}$ for these aeroelastic

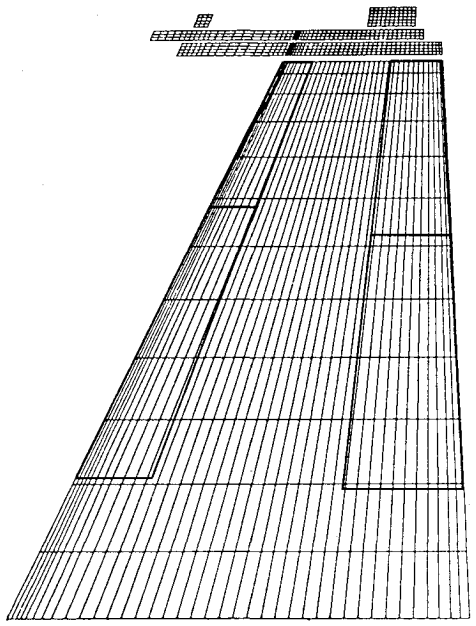

Fig. 17 F/A-18 CAP-TSD wing and tip missile with computational grid.

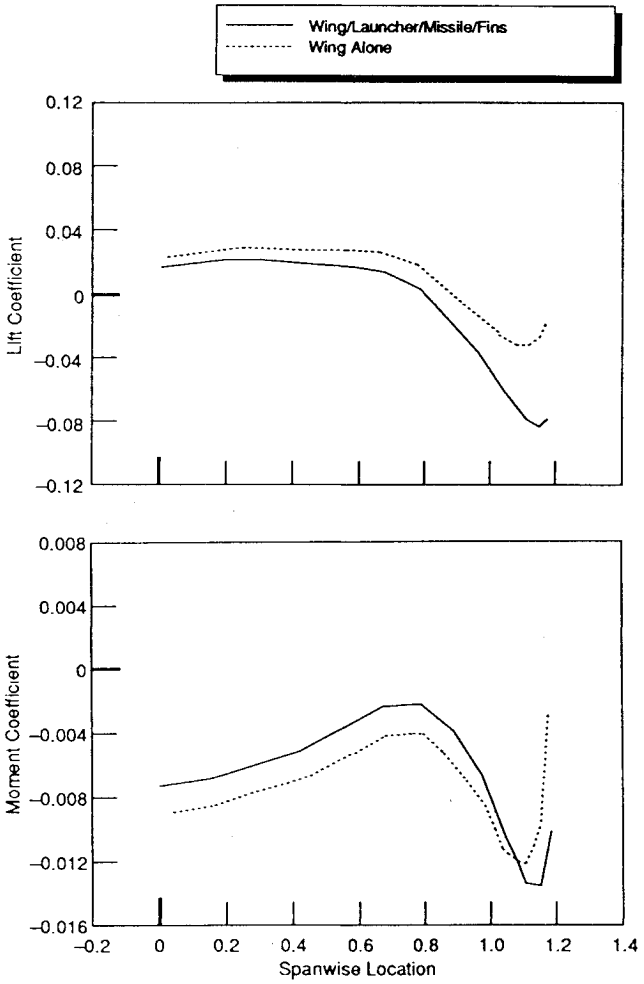

Fig. 18 Comparison of XTRAN3S and CAP-TSD spanwise C_l and $C_{(1/4)m}$ distributions for wing-alone and wing with tip missile computed using the nonlinear TSD equation and a rigid representation of the structure.

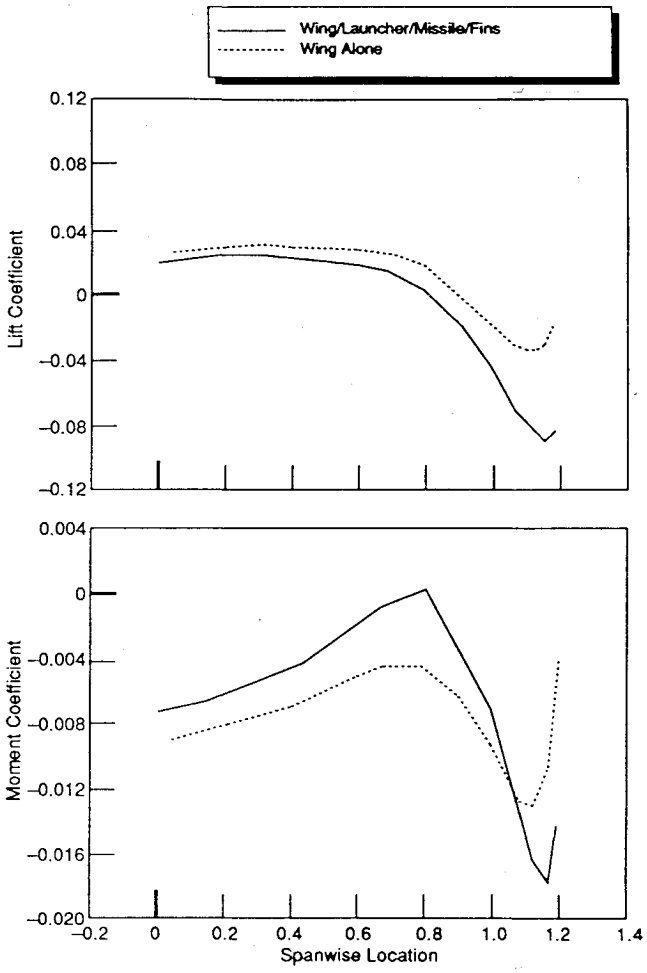

Fig. 19 Comparison of XTRAN3S and CAP-TSD spanwise C_l and $C_{(1/4)m}$ distributions for wing-alone and wing with tip missile computed using the nonlinear TSD equation and a flexible representation of the structure.

solutions. The lift distributions display similar trends as obtained from the data when modeling the rigid structure (Fig. 18). However, the spanwise flexible $C_{(1/4)m}$ is different from the data for the rigid structure in that the tip missile flexible $C_{(1/4)m}$ goes to zero at $\eta = 0.8$ and has a larger maximum negative value -0.018 at $\eta = 1.15$. Also, it can be seen that flexibility effects change the shape of the $C_{(1/4)m}$ curve for the full configuration case. The differences are due to the aerodynamics of the launcher, tip missile, and missile fins.

Linear and nonlinear dynamic aeroelastic analyses were performed for the F/A-18 tip missile case for the conditions $M_\infty = 0.8986$, $\alpha_m = 0.4396$ deg, $q_\infty = 29.7$ psi, and $V_\infty = 1122.9$ kt. The addition of the tip missile and launcher resulted in a larger amplitude oscillation when compared to the wing-alone results. A more extensive narration of the F/A-18 nonlinear dynamic aeroelastic results is presented in Ref. 4.

Conclusions

The application of two unsteady transonic small-disturbance codes, XTRAN3S and CAP-TSD, for aeroelastic analysis of realistic fighter geometries was presented and discussed. The XTRAN3S code was used to investigate the wing-alone flutter speeds of the F-15 and F/A-18 aircraft, whereas the CAP-TSD code was used to calculate the flutter characteristics of the F-15 S/MTD and the F/A-18 wing with tip missile.

The calculations performed using the linearized TSD equation agreed well with the traditional aeroelastic analysis techniques using doublet lattice aerodynamics. However, when compared to the results computed using the nonlinear TSD

equation, significant changes to both flutter speeds and the amount of wing deformation were shown. In the case of the F-15 wing, roughly a 100-kt decrease in the flutter speed was computed, whereas the results for the F/A-18 wing indicated over a 100-kt increase in the flutter speed. These changes emphasize the importance of nonlinear aerodynamics to a transonic aeroelastic analysis. It was also shown that modeling multiple lifting surfaces or wingtip stores in the analyses produced significantly larger flutter responses than the comparable wing-alone solutions when using either linear or nonlinear aerodynamics.

Transonic small-disturbance theory is well suited for the analysis of the thin-winged F-15 and F/A-18 aircraft due to the moderate angles of attack and minimal viscous effects in the cases previously discussed. The XTRAN3S and the CAP-TSD codes provide an efficient means of performing a nonlinear aeroelastic study because of their relatively low computational cost and simplicity of the gridding. These are distinct advantages over using other fluid dynamic methods based on higher-order aerodynamic theories. For general applicability, the CAP-TSD code is perferred over the XTRAN3S code because of its ability to treat complex configurations and its flexible input data structure.

The time-marching aeroelastic analysis procedure used within each code results in a series of generalized displacement time histories—one for each structural mode. To interpret these results, some type of parametric identification technique must be used, i.e., phase plane plotting in conjunction with curve fitting of the time histories using complex exponential functions. Currently, these techniques are time consuming and user intensive; therefore, future work must involve automating these procedures.

The aeroelastic calculations performed for this research involve simple three or five mode idealizations of the wing structural dynamics that, for fighter applications, are not adequate for an aircraft flutter analysis. More representative structural models consist of a range from 10 to 40 vibratory modes. However, routinely performing a stability analysis of a 40-mode coupled system by curve fitting each generalized displacement time history is impractical due to the enormous work required. Additionally, there is a significant preprocessing effort associated with spline fitting each vibratory mode shape for the input data. Therefore, a great deal of work is needed to integrate the TSD codes into a cost/time efficient engineering environment.

Acknowledgments

This work was performed under Contract F3 3615-87-C-3212 for the Aeroelastic Group, Analysis and Optimization Branch of the Structures Division, Flight Dynamics Laboratory, Air Force Wright Aeronautical Laboratories, Wright-Patterson Air Force Base, Ohio. The Air Force project engineers were Larry J. Huttsell and Mark R. Lee.

References

[1]Borland, C. J., and Rizzetta, D. P., "Transonic Unsteady Aerodynamics for Aeroelastic Applications," Vol. 1, AFWAL-TR-80-3107, Air Force Flight Dynamics Lab., Air Force Wright Aeronautical Labs., Wright-Patterson AFB, OH, June 1982.

[2]Batina, J. T., "An Efficient Algorithm for Solution of the Unsteady Transonic Small-Disturbance Equation," AIAA Paper 87-0109, Jan. 1987.

[3]Giesing, J. P., and Kalman, T. P., "Subsonic Steady and Oscillatory Aerodynamics for Multiple Interfering Wings and Bodies (Production Engineering User's Manual)," McDonnell Douglas Corp., MDC-J7295, St. Louis, MO, Oct. 1976.

[4]Pitt, D. M., Drouin, D. V., and Fuglsang, D. F., "Applications of XTRAN3S and CAP-TSD to Fighter Aircraft," Wright Research and Development Center, WRDC-TR-89-3048, Wright-Patterson AFB, OH.

[5]Rizetta, D. P., "Time-Dependent Response of a Two-Dimensional Airfoil in Transonic Flow," *AIAA Journal*, Vol. 17, No. 1, 1979, pp. 26–32.

[6]Edwards, J. W., Bennett, R. M., Whitlow, W., Jr., and Siedel, D. A., "Time-Marching Transonic Flutter Solutions Including Angle-of-Attack Effects," *Journal of Aircraft*, Vol. 20, No. 11, 1983, pp. 899–906.